DEM-Aided Block Adjustment for Satellite Images With Weak Convergence Geometry

Tee-Ann Teo, Liang-Chien Chen, Chien-Liang Liu, Yi-Chung Tung, and Wan-Yu Wu

***Abstract*—To acquire the largest possible coverage for environmental monitoring, it is important in most situations that the overlapping areas and the convergent angles of respective satellite images be small. The traditional bundle adjustment method used in aerial photogrammetry may not be the most suitable for direct orientation modeling in situations characterized by weak convergence geometry. We propose and compare three block adjustment methods for the processing of satellite images using the digital elevation model (DEM) as the elevation control. The first of these methods is a revised traditional bundle adjustment approach. The second is based on the direct georeferencing approach. The third is a rational function model with sensor-oriented rational polynomial coefficients. A collocation technique is integrated into all three methods to improve the positioning accuracy. Experimental results indicate that using the DEM as an elevation control can significantly improve the geometric accuracy as well as the geometric discrepancies between images. This is the case for all three methods. Moreover, the geometric performance of the three methods is similar. There is a significant improvement in geometric consistency between overlapping SPOT images with respect to single image adjustment for steep areas.**

***Index Terms*—Digital elevation model (DEM), direct georeferencing, modified bundle adjustment, rational function model (RFM).**

I. Introduction

ONE of the most important applications of satellite images is for landuse/landcover monitoring. It is the case that, due to satellites' small field of view (FOV), the area of interest often covers two or more images. Thus, mosaicking becomes a must. Another important application of remotely sensed images is detection of change. In this case, multitemporal images should be registered before performing the comparison. Simultaneous block adjustment is the preferred approach to enhancing the quality of this geometric registration. The adjusted orientation parameters provide a sound foundation for rigorous orthorectification. Except for those satellites that are dedicated to digital elevation model (DEM) generation (such as ALOS-PRISM, ASTER, Cartosat-1, SPOT-5 HRS, etc.), it is observed that to acquire the largest possible coverage, the area of overlap of the satellite images should generally be small. In addition, it should be noted that the convergent angles for a stereo model are not always large.

Block adjustment can enhance the geometric consistency between satellite images to increase the accuracy for orientation determination [1]. There are three types of adjustment approaches, namely, bundle adjustment [2]–[4], direct georeferencing [5]–[7], and the rational function model (RFM) [8].

From the photogrammetric point of view, traditional 3-D bundle adjustment is the most mature approach in that the collinearity condition for all of the tie points (TPs) and ground control points (GCPs) are satisfied simultaneously. However, due to the small scene size of the satellites, favorable convergence geometry cannot always be expected. In addition, the area of overlap between satellite strips may not be always large enough. Hence, the bundle adjustment approach needs to be modified to adopt for the weakly convergence geometry.

Orun and Natarajan [9] use collinearity equations and second-order polynomials to describe the dynamic sampling of a linear charge-coupled device (CCD) sensor. The bundle adjustment method is applied to study the SPOT geometry. Their experimental results indicate that a smaller angle of convergence has a significant effect on the elevation accuracy. A weakly convergent angle (i.e., 10°) may cause an elevation error of hundreds of meters.

In direct georeferencing, on the other hand, orbital and attitude data are utilized for orientation modeling. There are increasing amounts of on-board data available due to advances in geographic positioning system (GPS), inertial navigation system (INS), and star tracker technology. Orbital and attitude data provide relatively accurate position and attitude information. Thus, the number of GCPs required for direct georeferencing could be reduced. However, to preserve the accuracy of image parts within the overlapping area of connecting strips, TPs need to be included. Again, some improvements should be added to cope with cases where there is weakly convergence geometry or small overlap.

Due to its simplicity of implementation and standardization, RFM has been widely used in the field of remote sensing. In the RFM, one uses the ratio of two cubic polynomials and the rational polynomial coefficients (RPCs), which are determined by fitting the physical camera model to describe the relationship between object space and image space [10]. To some extent, the RFM may be interpreted as another form of direct

Manuscript received March 12, 2009; revised July 23, 2009. First published November 24, 2009; current version published March 24, 2010. This work was supported in part by the National Science Council and in part by the National Land Surveying and Mapping Center of Taiwan.

T.-A. Teo is with the Department of Civil Engineering, National Chiao Tung University, Hsinchu 300, Taiwan (e-mail: tateo@mail.nctu.edu.tw).

L.-C. Chen and C.-L. Liu are with the Digital Photogrammetry Laboratory, Center for Space and Remote Sensing Research, National Central University, Taoyuan 32001, Taiwan (e-mail: lcchen@csrsr.ncu.edu.tw; ericleo@csrsr.ncu.edu.tw).

Y.-C. Tung is with the CECI Engineering Consultants, Inc., Taipei 10637, Taiwan (e-mail: 92322094@cc.ncu.edu.tw).

W.-Y. Wu is with the Kingwaytek Technology Company, Ltd., Taipei 10084, Taiwan (e-mail: 953202072@cc.ncu.edu.tw).

Color versions of one or more of the figures in this paper are available online at http://ieeexplore.ieee.org.

Digital Object Identifier 10.1109/TGRS.2009.2033935

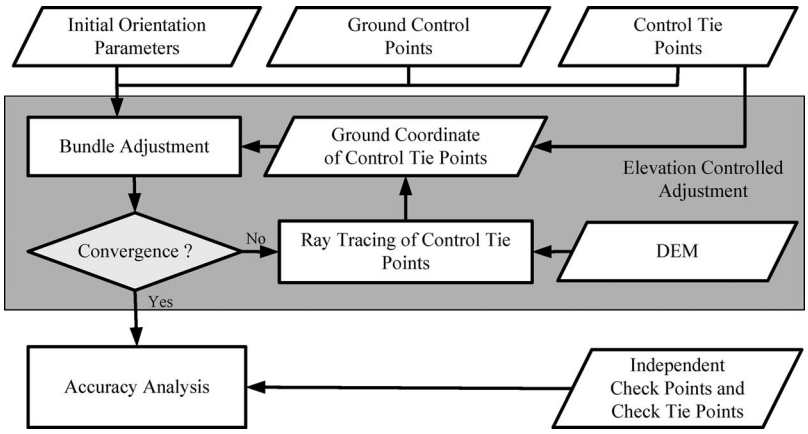

Fig. 1. Workflow of elevation control for bundle adjustment.

georeferencing when RPCs are derived from the quality onboard orientation parameters. For some high-resolution satellite images, IKONOS for instance, RPCs are provided rather than the original orientation parameters. Thus, the same problem occurs again for those image blocks with weak convergence geometry.

The major applications for remotely sensed images are for the detection of natural resources and monitoring of the geoenvironment. To acquire the largest possible coverage, the area of overlap of satellite images should be as small as possible. However, weak geometry of the area of intersection will lead to a large elevation error. In other words, the base-to-height ratio of multiorbit satellite images is, frequently, not large enough. Although several investigators have discussed block adjustment methods for images with good geometric convergence (e.g., see ALOS PRISM [11], ASTER [12], [13], IKONOS in-track stereo [14], and SPOT-5 HRS [1]), block adjustment with low overlap from weakly convergence geometry satellite images has seldom been discussed.

The main objective of this investigation is to propose a solution to solve the problem of weakly convergence geometry for satellite image blocks. Toutin [15] used elevation-added TPs in their method for block adjustment. The elevation of the TP is fixed to avoid the vertical error caused by weak convergence geometry. Since the planimetric coordinate of the TP is still unknown in the solution, the height of the TP is not easy to determine automatically. It is assumed that a DEM is available to provide a solution. We include an existing DEM in block adjustment. Hence, the height of the TP must be iteratively interpolated from the DEM in the block adjustment process. Since the final goal is to produce orthoimages for landuse/landcover monitoring rather than 3-D surface reconstruction, the assumption of the availability of DEM is justified. In this investigation, we propose a revised block adjustment procedure including DEMs as elevation controls. Least squares collocation is integrated in the solution to compensate for systematic errors.

Three types of the block adjustment methods, namely, bundle adjustment, direct georeferencing, and RFM, are proposed in this investigation.

In the modified bundle adjustment method, there are three groups of observation equations including image coordinates with the collinearity condition, orientation parameters, and ground coordinates. Next, an elevation-controlled mechanism is proposed, which uses a DEM. The mechanism operates in such a way that the ground coordinates are iterated until simultaneously satisfying the collinearity condition, the ground surface, and the weighted orientation parameters. Finally, least squares collocation is included to adjust for local systematic errors.

In direct georeferencing, the observation vectors for the GCPs and TPs are formulated first. Preliminary fitting of the orbital parameters is employed when calculating all discrepancies for GCPs and the disparities for TPs. The discrepancy/parallax vectors are then employed for least squares collocation.

For implementation of elevation control in an RFM, a typical block adjustment is developed first. Since the RPCs are derived from precise GPS, INS, and star tracker data, they can be treated as constants. The block adjustment process necessitates the use of affine transformation and the observation equations of 3-D ground coordinates. In the adjustment process, the DEM is used as an elevation control. The ground coordinates are iterated until simultaneously satisfying the RFM, ground surface, and the weighted ground coordinates. Again, a least squares collocation is included.

II. Proposed Scheme

The proposed scheme is comprised of the following three adjustment models: 1) modified bundle adjustment; 2) the direct georeferencing model; and 3) the RFM. The details of each model are given below.

A. Modified Bundle Adjustment

The modified bundle adjustment process includes two major parts. In the first, the bundle adjustment model is established. In the second part, bundle adjustment is carried out using the DEM as an elevation control. Fig. 1 illustrates the work flow for DEM elevation control using bundle adjustment.

Before performing bundle adjustment, we transform the orientation parameters and object coordinates into a work coordinate system that is related to the tangential coordinate system [16]. The origin is set at the centroid of the GCP to avoid

numerical instability or projection error caused by a long track. In addition, the high correlation between orbital parameters and attitudes can be better depicted and separated during weighting.

The collinearity condition equations state that the exposure station, any object points, and its image point all lie along a straight line. The equations are modified, as in (1), to fit the imaging geometry of the satellite images. The exterior orientation parameters, including orbital and attitude, are characterized by second-order polynomials as functions of sampling time t relative to the first scan line [17], i.e.,

$$x_i = -f\frac{m_{11t}(X_i-X_t^c)+m_{12t}(Y_i-Y_t^c)+m_{13t}(Z_i-Z_t^c)}{m_{31t}(X_i-X_t^c)+m_{32t}(Y_i-Y_t^c)+m_{33t}(Z_i-Z_t^c)}$$

$$S_y \cdot y_i = -f\frac{m_{21t}(X_i-X_t^c)+m_{22t}(Y_i-Y_t^c)+m_{23t}(Z_i-Z_t^c)}{m_{31t}(X_i-X_t^c)+m_{32t}(Y_i-Y_t^c)+m_{33t}(Z_i-Z_t^c)} \tag{1}$$

where

x_i, y_i	photocoordinates at point i;
X_i, Y_i, Z_i	object coordinates at point i;
S_y	scale affinity of CCD size;
f	focal length;
X_t^c, Y_t^c, Z_t^c	exterior orbital parameters at time t;
$m_{11t}, \ldots, m_{33t}$	rotation matrix from attitude parameters at time t.

To distinguish the correlation between exterior orientation parameters, we include the pseudoequation and use *a priori* information for weighting. The pseudoequations [2] include the exterior orientation parameters and ground coordinates. Finally, the observation equation, pseudoequation for the exterior orientation parameter, and pseudoequation for the ground coordinates are combined. A least squares adjustment technique is applied to solve the unknown parameters. An in-depth description of the bundle adjustment can be found in [2].

The ray tracing technique is modified from [2] to determine the ground position of a TP. The ray tracing of the proposed bundle adjustment assumes that the orientation parameters, the DEM, and the coordinates of point are available. Since the orientation parameters are to be determined with the integration of the ray tracing, an iteration process is needed. This iterative procedure is used to determine the intersection point between the ray and the ground surface. The following are the three major processes in ray tracing: 1) calculation of the planimeter coordinates (X, Y) for an initial elevation Z; 2) interpolation of the new elevation Z' from the DEM according to planimeter coordinates (X, Y); and 3) using interpolated elevation Z' as the approximation value for the next iteration of the block adjustment. The iteration proceeds until the elevation variation is small enough.

After the ray tracing, the locations resulting from different orbits for the same TPs are not coincident. We take the average position of two ground points as the initial position of this TP. The weak geometry of the intersection gives rise to elevation errors that can be overcome by using DEM recursively during the least squares adjustment. Referring to Fig. 2, we see that the elevation Z without prime denotes the elevation after bundle adjustment, and the Z with prime denotes the elevation after interpolation in DEM. The subscripts of Z indicate the number of iterations. The computation procedure starts from the initial value of Z_1 to Z_1', moving to Z_2 and Z_2', and so forth until convergence. This way, we can control elevation error within a reasonable range where convergence is expected.

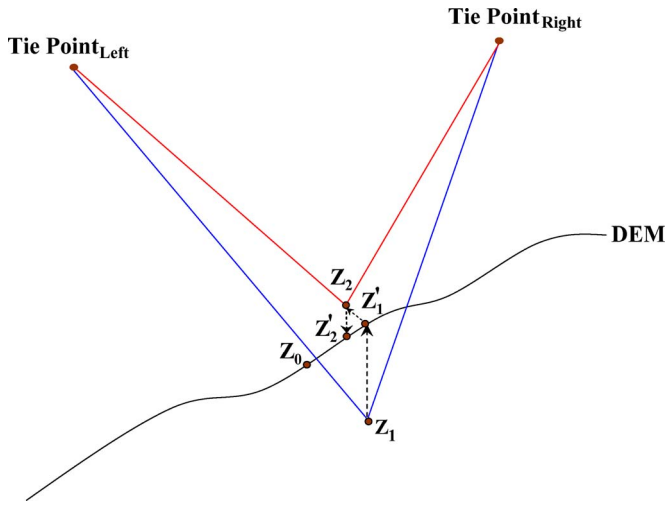

Fig. 2. DEM elevation control.

B. Direct Georeferencing

The direct georeferencing model comprises two major parts. In the first part, preliminary orbit fitting using the GCPs is carried out. In the second part, the orbit is refined by least squares collocation with TPs. A DEM is used as an elevation control in the block adjustment procedure. Fig. 3 illustrates the work flow of block adjustment with elevation control.

The satellite on-board data include orbital parameters and attitude data. We use the data to establish the state vectors of satellite position and the line of sight [18]. The state vectors are illustrated in Fig. 4. The collinearity condition equation for the state vectors is shown in (2). Once the exterior orientation parameters are modeled, the corresponding ground coordinates for an image pixel can be calculated. The GCPs are used to adjust the orbital parameters. Equation (3) is the collinearity equation with preliminary orbit fitting. To compensate the error for orbital parameters, a low-degree polynomial is applied in this state. We have

$$\vec{G} - \vec{P} = S\vec{U} \tag{2}$$

$$\vec{G} - (\vec{P} + \Delta\vec{P}) = S\vec{U} \tag{3}$$

where

$\vec{G}$	ground point vector;
$\vec{P}$	satellite position vector;
$\vec{U}$	satellite line-of-sight vector;
S	scale factor;
$\Delta\vec{P}$	orbital polynomial function.

Geometric consistency is maintained between images by utilizing residual vectors on the TPs to reduce the image discrepancy. Thus, we need to compute the residual vectors for TPs.

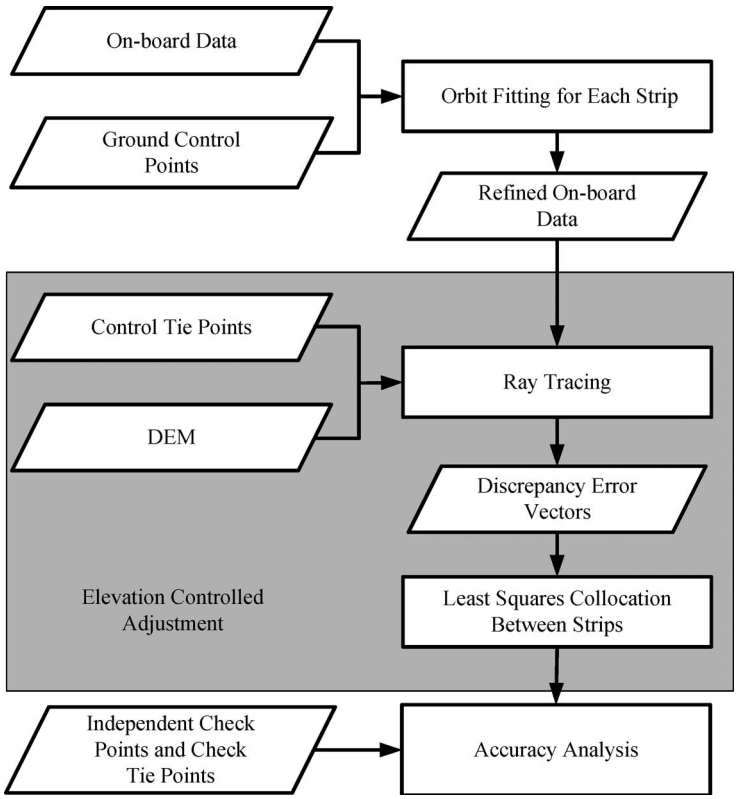

Fig. 3. Workflow of block adjustment for direct georeferencing.

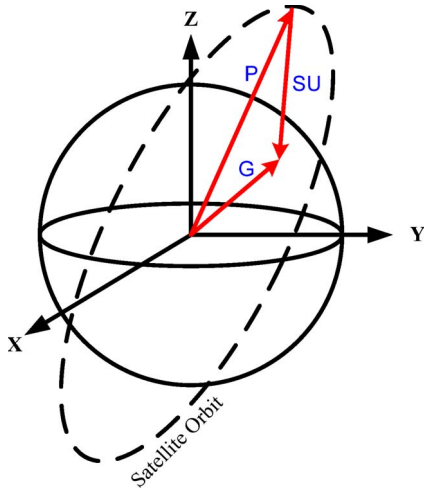

Fig. 4. State vectors.

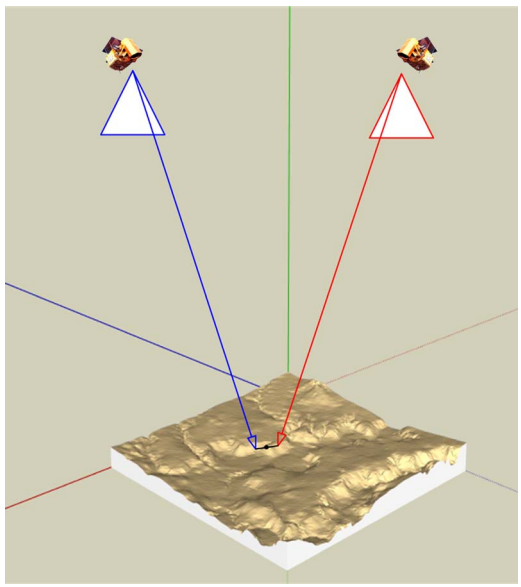

Fig. 5. Error vector on TP.

First, we use the orbital parameters and the image coordinates of a TP to calculate the line of sight. Given a DEM, the ray tracing technique is then applied to determine the ground position of a TP. The following are the three major processes in ray tracing: 1) calculation of the planimeter coordinates (X, Y) for an initial elevation Z; 2) interpolation of the new elevation Z' from the DEM according to planimeter coordinates (X, Y); and 3) using interpolated elevation Z' as the approximation value for the next iteration until the distance between intersection point and DEM is convergent. The procedure is repeated for its counterpart in the other image. As can be seen in Fig. 5, there are two ground corresponding points for each pair of TPs. This indicates discrepancy between the images. The center of two ground points is used as a constraint. The residual vector for each TP is the vector from one ground position to the middle of the two points.

Block adjustment is carried out by employing the discrepancy vectors of these TPs in a least squares collocation. The results after least squares collocation are shown in Fig. 6. In the

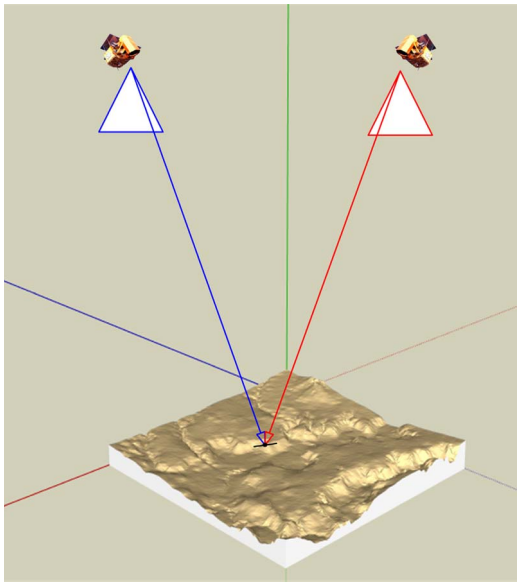

Fig. 6. Results of collocation on TP.

process, we assume that the x, y, and z axes are independent. Three 1-D functions are applied to adjust the orbit. The model of least squares collocation [19] is shown in the following equation:

$$S_k = \sigma_k \bullet \Sigma_k^{-1} \bullet l_k \tag{4}$$

where

k x, y, and z axes;
S_k correct value of the interpolated point;
σ_k row covariance matrix for the interpolated point with respect to the TPs;
Σ_k covariance matrix for the TPs;
l_k residual vectors for the TPs.

To determine the value of the covariance matrix, we select a Gaussian function with some empirical values for the covariance function [19], as shown in the following equation:

$$C = \left\{ \begin{array}{ll} (1-r_n)\,\mu_k \exp^{-\left(2.146\frac{d}{d_{\max}}\right)^2}, & if\ d \neq 0 \\ \mu_k, & if\ d = 0 \end{array} \right\} \tag{5}$$

where

C element of covariance matrix;
d distance between intersection point and TP;
$d_{\max}$ maximum distance of intersection point;
μ_k variance of TPs' residual;
r_n filtering ratio, in which we use 0.2 in the experiment.

This empirical value 2.146 is selected so that the covariance limit is $1\% * (1 - r_n)\mu_k$ when $d = d_{\max}$.

C. RFM

The proposed method is also composed of two parts, namely, RFM-based block adjustment, and elevation control with DEM.

The RFM uses the ratio of two cubic polynomials to the RPCs. The RPCs are determined by fitting the physical camera model to describe the relationship between object space and image space [20]. To maintain numerical precision, the object and image space coordinates will be normalized to $(-1, +1)$. General forms of RFM can be written as

$$x = \frac{\sum_{i=0}^{m1}\sum_{j=0}^{m2}\sum_{k=0}^{m3} c_{ijk} X^i Y^j Z^K}{\sum_{i=0}^{n1}\sum_{j=0}^{n2}\sum_{k=0}^{n3} d_{ijk} X^i Y^j Z^K}$$

$$y = \frac{\sum_{i=0}^{m1}\sum_{j=0}^{m2}\sum_{k=0}^{m3} e_{ijk} X^i Y^j Z^K}{\sum_{i=0}^{n1}\sum_{j=0}^{n2}\sum_{k=0}^{n3} f_{ijk} X^i Y^j Z^K} \tag{6}$$

where

x, y image coordinates;
X, Y, Z object coordinates;
c_{ijk}, d_{ijk}, e_{ijk}, f_{ijk} polynomial coefficients.

The coefficients of the RFM are called RPCs. Typically, since the RPCs are selected to the third degree, 80 coefficients are essentially included. There are two approaches for determining the RPCs. The first one is the *GCP-derived RPC* approach in which the coefficients are derived from numerous GCPs. However, this approach requires too many GCPs and, therefore, is considered unrealistic. The second option is the *sensor-oriented RPC* approach, which utilizes the on-board orientation of the satellite, including the orbital parameters and attitude data to generate enough transformation anchor points. This method can achieve high precision provided the on-board orbital parameters and attitude data are accurate. As most high-resolution satellites are equipped with instruments such as GPS, INS, and star trackers, they are capable of providing satisfactory orientation measurements. Accordingly, sensor-oriented RPCs are employed in this investigation. Fig. 7 illustrates the work flow of RFM block adjustment with elevation control.

To compensate for the systematic bias of the RPCs, we use an affine transformation to correct the error in the image space [21], [22]. The affine model is used to compensate the original image space and RFM's image space. As the RPCs are calculated from the on-board data, the quality of RPCs is referred to the quality of on-board data. Due to the small FOV (e.g., SPOT is 4°) and the high precision of RPCs, the displacements in a small area may be assumed to be linear. Hence, an affine transformation might be applied to compensate the bias between original image space and RFM's image space. The coefficients for the affine transformation can be calculated from the GCPs. The equation for the affine transformation is

$$\begin{aligned} S_{\mathrm{GCP}} &= a_0 + a_1 \cdot S_{\mathrm{RFM}} + a_2 \cdot L_{\mathrm{RFM}} \\ L_{\mathrm{GCP}} &= b_0 + b_1 \cdot S_{\mathrm{RFM}} + b_2 \cdot L_{\mathrm{RFM}} \end{aligned} \tag{7}$$

where

S_{GCP}, L_{GCP} image coordinates of the GCP;
S_{RFM}, L_{RFM} image coordinates determined by RFM;
$a_0 \sim b_2$ affine coefficients.

The least squares form of the RFM equations can be represented in matrix form, as in (8). In turn, the matrix form can be

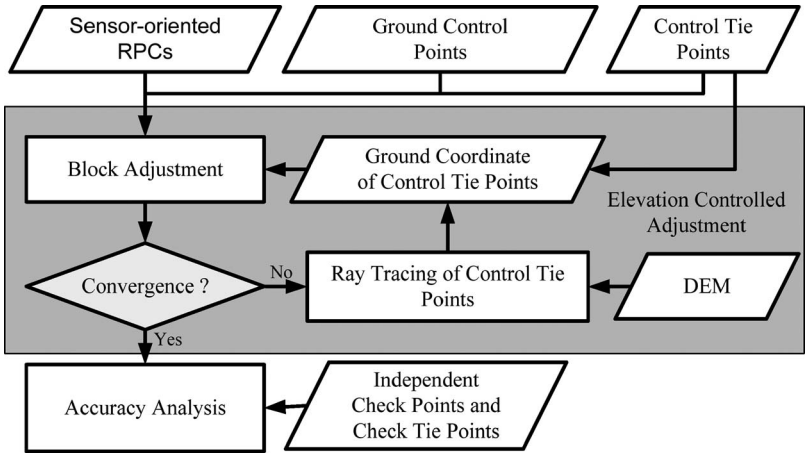

Fig. 7. Workflow of elevation control for RFM.

represented in a compact matrix notation as

$$\begin{bmatrix} v_{sij} \\ v_{lij} \end{bmatrix} + \begin{bmatrix} \frac{\partial F_{sij}}{\partial a_{0j}} & \frac{\partial F_{sij}}{\partial a_{1j}} & \frac{\partial F_{sij}}{\partial a_{2j}} & 0 & 0 & 0 \\ 0 & 0 & 0 & \frac{\partial F_{lij}}{\partial b_{0j}} & \frac{\partial F_{lij}}{\partial b_{1j}} & \frac{\partial F_{lij}}{\partial b_{2j}} \end{bmatrix} \begin{bmatrix} \delta a_{0j} \\ \delta a_{1j} \\ \delta a_{2j} \\ \delta b_{0j} \\ \delta b_{1j} \\ \delta b_{2j} \end{bmatrix} + \begin{bmatrix} \frac{\partial F_{sij}}{\partial X_i} & \frac{\partial F_{sij}}{\partial Y_i} & \frac{\partial F_{sij}}{\partial Z_i} \\ \frac{\partial F_{lij}}{\partial X_i} & \frac{\partial F_{lij}}{\partial Y_i} & \frac{\partial F_{lij}}{\partial Z_i} \end{bmatrix} \begin{bmatrix} \delta X_i \\ \delta Y_i \\ \delta Z_i \end{bmatrix} = \begin{bmatrix} -F^0_{sij} \\ -F^0_{lij} \end{bmatrix} \tag{8}$$

$$V_{ij} + B'_{ij}\Delta'_j + B''_{ij}\Delta''_i = \varepsilon_{ij} \tag{9}$$

where

V_{ij} residual matrix for the RFM equations;
B'_{ij}, B''_{ij} observation matrices for the RFM equations;
Δ'_i, Δ''_j matrix of unknown parameters;
ε_{ij} approximation matrix;
i number of points;
j number of images.

Block adjustment can enhance the geometric consistency between the images to improve their accuracy for orientation determination. The observation equations for the RFM and object coordinates are included in the block adjustment process. Since the affine coefficients are not highly correlated, we only include the pseudoobservation equations for the object coordinates, without doing this for the affine coefficients. The pseudoequation for ground coordinates is formulated in (10). The matrix form of (10) is represented in a compact matrix notation as

$$\begin{bmatrix} V_{X_i} \\ V_{Y_i} \\ V_{Z_i} \end{bmatrix} - \begin{bmatrix} \delta X_i \\ \delta Y_i \\ \delta Z_i \end{bmatrix} = \begin{bmatrix} dX_i \\ dY_i \\ dZ_i \end{bmatrix} \tag{10}$$

$$V''_i - \Delta''_i = C''_i \tag{11}$$

where

V''_i residuals matrix for the pseudoequation;
Δ''_i matrix of unknown parameters;
C''_i approximation matrix of measurement.

The combined observation equations can be written as (12). The weight matrix is shown in (13). The weight of the image coordinate is determined by the priori standard error of the image coordinate. We use 0.5 pixels as the standard error in this investigation. The weight of the ground coordinate is related to the standard error of the control point and TP. The standard error of the control point is referred to the measurement accuracy. The standard error of TP is ten times the control point. We have

$$\begin{bmatrix} V \\ V'' \end{bmatrix} + \begin{bmatrix} B' & B'' \\ 0 & -I \end{bmatrix} \begin{bmatrix} \Delta' \\ \Delta'' \end{bmatrix} = \begin{bmatrix} \varepsilon \\ C'' \end{bmatrix} \tag{12}$$

$$W = \begin{bmatrix} W' & 0 \\ 0 & W'' \end{bmatrix} \tag{13}$$

where

V, V'' residuals matrix;
B', B'' observation matrix for the equations;
Δ', Δ'' matrix of unknown parameters;
ε, C'' approximation matrix of measurements;
W' weight of the image coordinate;
W'' weight of the ground coordinate.

Due to the weak convergence, a DEM is also included in the block adjustment as an elevation control. The idea of this elevation control is same as the modified bundle adjustment procedure. First, using the new planimetric coordinates (X, Y) for each block adjustment iteration, we interpolate a new elevation Z' from the DEM and apply the elevation Z' for the next iteration of the block adjustment. Through iteration and interpolation, we attain an accurate result and overcome the problem of elevation error.

D. Accuracy Analysis

Four types of points, namely GCPs, control TPs, independent check points (ICPs) and independent check TPs (ICTPs), are included in the validation. After block adjustment, we use ICPs and ICTPs for accuracy analysis. The ICPs are used to check the

absolute accuracy as the ground coordinates of points are available. We use the orientation parameters, image coordinates, and height of ICP to calculate the ground coordinates. The difference between calculated and actual ground coordinates are used to evaluate the absolute accuracy of image.

The role of ICTPs is to evaluate the relative accuracy between images. An ICTP delivers image coordinates in two images. Each image coordinate may calculate a ground coordinate using the ray tracing technique with a DEM. The distance between these two ground coordinates can evaluate the relative accuracy between images. We also calculate the root mean square error (RMSE) of ICPs and ICTP as the indices for accuracy analysis.

The result of single adjustment is also provided to compare the performance of single and block adjustments. The DEM is not needed for single adjustment. The single adjustment performs the geometric correction strip by strip. The block adjustment performs the adjustment for strips simultaneously. Since the single adjustment uses GCPs only, there is no need for a DEM. In the modified bundle adjustment, the single adjustment uses collinearity equations with GCP to calculate the orientation parameters without using TP and pseudoequations. In the direct georeferencing, the single adjustment uses state-vector collinearity equations with GCP to calculate the unknown parameters without using TP or least squares collocation. In the RFM, the single adjustment uses affine transformation with GCP to calculate the unknown parameters without using TP and pseudoequations.

III. Experimental Result

The test data include three SPOT 5 supermode panchromatic image strips. In each experiment, we test two cases, with different numbers of scenes. Case I contains one standard scene per strip, while case II contains two. The test areas are in the center part of Taiwan stretching from the west coast to the east coast, as shown in Fig. 8(a) and (b). The strips have about 10%–15% overlap, as shown in the figure. GCPs and ICPs are acquired from 1 : 5000 scaled topographic maps. GCP accuracy is estimated to be better than 3 m. The TPs and ICTPs are acquired by manual measurements. The terrain of the test site has about 3800 m relief, as shown in Fig. 8(c) and (d). The vertical accuracy of DEM is estimated at about 3 m for nonhilly area. The vertical accuracy in the hilly area could be large than the estimated value. Information related to the test images is given in Table I. Before the geometric correction, we use all the ground points to evaluate the accuracy of on-board data. Table II shows the mean error and RMSE of both cases. The accuracy is better than 50 m, which reflects the specifications of SPOT-5 [23].

The validation experiments are carried out in three parts. First, the geometrical consistency between strips is evaluated; second, the absolute accuracy is examined; and finally, mosaicked images generated from the derived orientation parameters are checked. In this section, the "Modified Bundle Adjustment," "Direct Georeferencing," and "RFM" are indicated by **MBA**, **DG**, and **RFM**, respectively. Since the SPOT image provides only on-board data, we generate 80 sensor-oriented RPCs for each of the SPOT images using the method in [24].

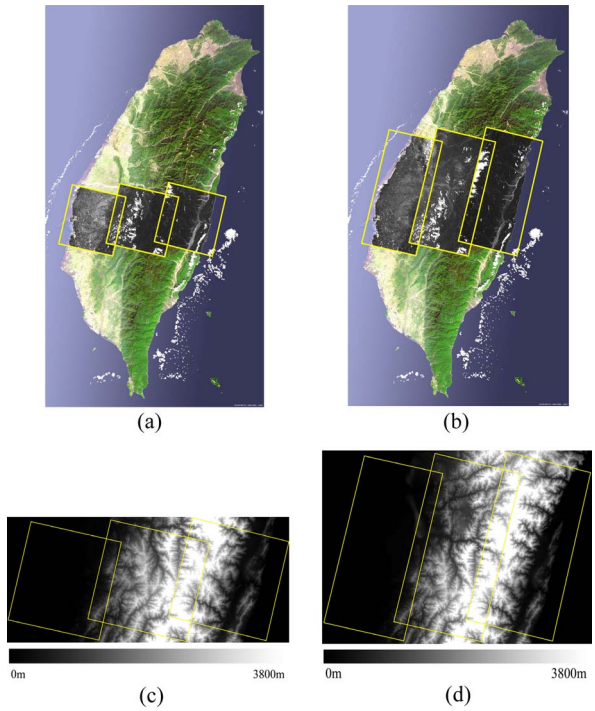

Fig. 8. Test images. (a) Case I. (b) Case II. (c) DEM of case I. (d) DEM of case II.

TABLE I
Information Related to Test Data

Description		Strip 1	Strip 2	Strip 3
Date		2003/6/21	2003/5/31	2003/7/1
Incidence Angle (Deg)		5.21°	5.65°	-14.76°
GSD (m)		2.52	2.52	2.67
Overlapping Area		10%		15%
Case I	Image Size	24000*24000(Supermode)		
	Number of GCPs	9	9	9
	Number of ICPs	25	11	11
	Number of TPs	19		13
	Number of ICTPs	18		13
Case II	Image Size	24000*48000(Supermode)		
	Number of GCPs	20	22	22
	Number of ICPs	48	31	28
	Number of TPs	32		26
	Number of ICTPs	31		26
DEM		40m Topographic Data Base of Taiwan		
Elevation Range		0m-3800m		

TABLE II
Absolute Accuracy Before Adjustment

Units: meters	Strip1		Strip2		Strip3	
Case I	**E**	**N**	**E**	**N**	**E**	**N**
Mean	16.02	29.09	-1.93	8.03	-18.77	36.73
RMSE	16.38	29.39	6.05	10.34	19.84	37.41
Case II	**E**	**N**	**E**	**N**	**E**	**N**
Mean	15.95	29.10	0.62	6.43	-17.15	37.65
RMSE	16.34	29.37	5.89	10.75	18.11	38.32

A. Geometrical Consistency Between Strips

Case I: We choose a pair of TPs that appear in two images. A pair of TPs delivers two image coordinates in two images. Each image coordinate may calculate a ground position using

TABLE III
COMPARISON OF GEOMETRICAL CONSISTENCY (CASE I)

Units: meters			Strips 1 & 2 No. TP=19 No.ICTP=18		Strips 2 & 3 No. TP=13 No.ICTP=13	
Types			RMSE			
			E	N	E	N
MBA	Block	TP	2.17	1.27	5.27	3.61
		ICTP	1.22	1.68	3.56	4.24
	Single	ICTP	11.56	8.72	28.37	25.01
	Improvement	ICTP	10.34	7.04	24.81	20.77
DG	Block	TP	2.10	1.51	5.90	4.95
		ICTP	2.55	1.83	2.72	5.00
	Single	ICTP	10.85	9.65	27.71	28.11
	Improvement	ICTP	8.30	7.82	24.99	23.11
RFM	Block	TP	2.69	1.74	6.40	4.26
		ICTP	2.68	1.90	6.01	4.92
	Single	ICTP	6.99	6.59	22.58	28.22
	Improvement	ICTP	4.31	4.69	16.57	23.30

ray tracing technique with DEM and orientation parameters. Hence, a pair of TPs may obtain two ground positions from two images. The ground positions of TP are checked using ICTPs. Distance between these two ground positions is used to evaluate the discrepancy. Table III illustrates the accuracy of the performance of the process of using ICTPs for single image adjustment and block adjustment. The error vector for strips 1 and 2 after block adjustment is shown in Fig. 9(a)–(c); the error vector for strips 2 and 3 is shown in Fig. 9(d)–(f). Triangles indicate TPs, while circles represent the ICTPs. It can be seen that the error vectors for the three proposed methods are very similar.

The RMSE for the ICTP for strips 1 and 2 prior to the block adjustment is larger than 6.5 m. After block adjustment, it is better than 2.7 m. For strips 2 and 3, RMSE of ICTP is improved from 22 and 28 m to 6 and 5 m in the east and north directions, respectively. Significant improvement of geometrical consistency is demonstrated when TPs are employed in the block adjustment. The range of improvement is from 4 to 24 m. The difference obtained with the three methods is less than 1 m (i.e., 0.4 pixels). This is the case for all strips after block adjustment except when the RFM is in the east direction (for strips 2 and 3) because of the tradeoff phenomenon in the block adjustment. The phenomenon reveals the balance of GCPs and TPs that makes the relative accuracy improved with marginal degradations of absolute accuracy.

Case II: In case II, there are two standard scenes in a strip. Hence, the total number is six standard scenes. The geometrical consistency between strips is checked by measuring the TPs. The numbers of TPs in the overlapping area are 32 for strips 1 and 2 and 26 for strips 2 and 3. The numbers of check TPs are 31 for strips 1 and 2 and 26 for strips 2 and 3. The adjustment results with and without block adjustment are shown in Table IV. The results of geometrical consistency without block adjustment using MBA and DG are very similar. Before block adjustment, the geometrical consistency of single strip adjustment is around 10 m for strips 1 and 2. The geometrical consistency between strips 2 and 3 is only around 18 m due to the hilly terrain. After block adjustment, the geometrical consistency of strips 1 and 2 has improved to 2.5 m and

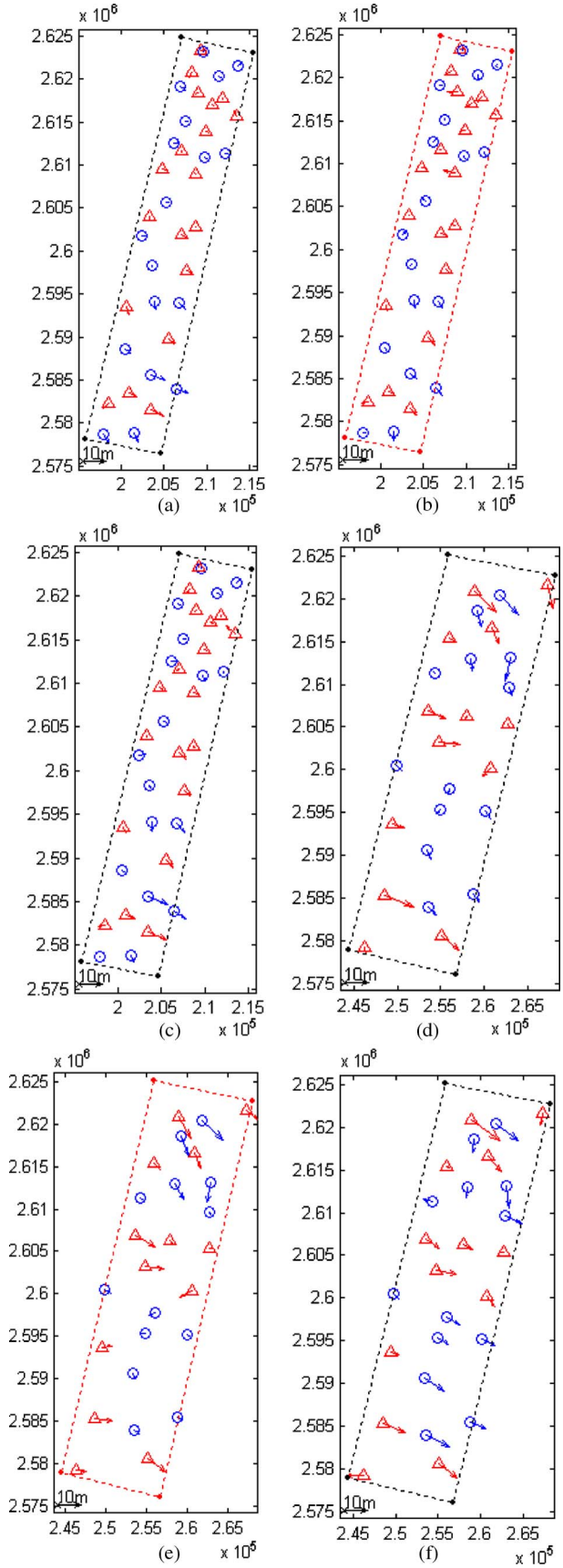

Fig. 9. Error vectors of geometrical consistency between strips (case I). (a) Strips 1 and 2 using DG. (b) Strips 1 and 2 using MBA. (c) Strips 1 and 2 using RFM. (d) Strips 2 and 3 using DG. (e) Strips 2 and 3 using MBA. (f) Strips 2 and 3 using RFM.

TABLE IV
COMPARISON OF GEOMETRICAL CONSISTENCY (CASE II)

Units: meters			Strips 1 & 2 No. TP=32 No.ICTP=31		Strips 2 & 3 No. TP=26 No.ICTP=26	
Types			RMSE			
			E	N	E	N
MBA	Block	TP	1.81	1.89	5.25	2.75
		ICTP	1.54	2.41	3.28	3.06
	Single	ICTP	6.76	9.34	16.70	16.39
	Improvement	ICTP	5.22	6.93	13.42	13.33
DG	Block	TP	1.83	2.09	5.45	3.78
		ICTP	2.08	2.39	3.22	4.12
	Single	ICTP	7.11	10.28	17.32	18.34
	Improvement	ICTP	5.03	7.89	14.10	14.22
RFM	Block	TP	2.36	2.14	7.00	3.82
		ICTP	2.41	2.50	5.18	4.30
	Single	ICTP	5.61	8.13	11.11	13.57
	Improvement	ICTP	3.20	5.63	5.93	9.27

TABLE V
COMPARISON OF ABSOLUTE ACCURACY FOR SINGLE IMAGE ADJUSTMENT (CASE I)

Units: meters	Strip1 No. GCP= 9 No. ICP = 25		Strip2 No. GCP= 9 No. ICP = 11		Strip3 No. GCP= 9 No. ICP = 11	
MBA	**RMSE E**	**RMSE N**	**RMSE E**	**RMSE N**	**RMSE E**	**RMSE N**
GCP	2.41	1.10	2.27	0.81	1.05	2.26
ICP	4.01	3.01	3.05	5.99	5.69	6.65
DG	**RMSE E**	**RMSE N**	**RMSE E**	**RMSE N**	**RMSE E**	**RMSE N**
GCP	2.78	1.49	2.51	1.82	1.33	2.72
ICP	4.05	3.11	3.13	6.00	5.60	6.25
RFM	**RMSE E**	**RMSE N**	**RMSE E**	**RMSE N**	**RMSE E**	**RMSE N**
GCP	3.84	1.67	3.76	2.62	2.79	3.83
ICP	3.70	2.58	3.58	6.33	5.99	6.44

the geometrical consistency between strips 2 and 3 is better than 4.5 m when MBA and DG are applied. The significant improvement of geometrical consistency shows the importance of using block adjustment. Note that the range of improvement is from 3 to 14 m.

The behavior of RFM is different from the other two methods. Although the results for geometrical consistency in single strip adjustment are better than the other methods, the RFM block adjustment results are less accurate.

B. Absolute Accuracy

Case I: The absolute accuracy is evaluated using ICPs. This test includes a comparison of the three proposed block adjustment methods. The results of single image adjustment are also provided for comparison. Table V shows the single image adjustment results obtained using each of the three methods. The numbers of GCPs and ICPs are also indicated. The result for strip 3 is around 7 m due to the 15° viewing angle and the high terrain relief. The absolute accuracy of strip 1 is better than that of strip 2 because the terrain relief is less extreme. The difference between these three methods is less than 1.8 m (i.e., 0.7 pixels) for all strips. Error vectors indicate no obvious

TABLE VI
COMPARISON OF ABSOLUTE ACCURACY WITH BLOCK ADJUSTMENT (CASE I)

Units: meters	Strip1 No. GCP= 9 No. ICP = 25 No. TP = 19		Strip2 No. GCP= 9 No. ICP = 11 No. TP = 32		Strip3 No. GCP= 9 No. ICP =11 No. TP = 13	
MBA	**RMSE E**	**RMSE N**	**RMSE E**	**RMSE N**	**RMSE E**	**RMSE N**
GCP	3.29	1.60	4.49	2.98	4.91	5.19
ICP	4.92	3.57	6.33	8.81	5.46	3.56
DG	**RMSE E**	**RMSE N**	**RMSE E**	**RMSE N**	**RMSE E**	**RMSE N**
GCP	3.58	2.64	5.68	2.78	5.55	7.74
ICP	4.48	2.71	6.39	8.38	5.45	3.22
RFM	**RMSE E**	**RMSE N**	**RMSE E**	**RMSE N**	**RMSE E**	**RMSE N**
GCP	3.68	1.95	3.39	2.16	5.51	6.20
ICP	4.47	2.54	4.45	8.24	5.94	3.57

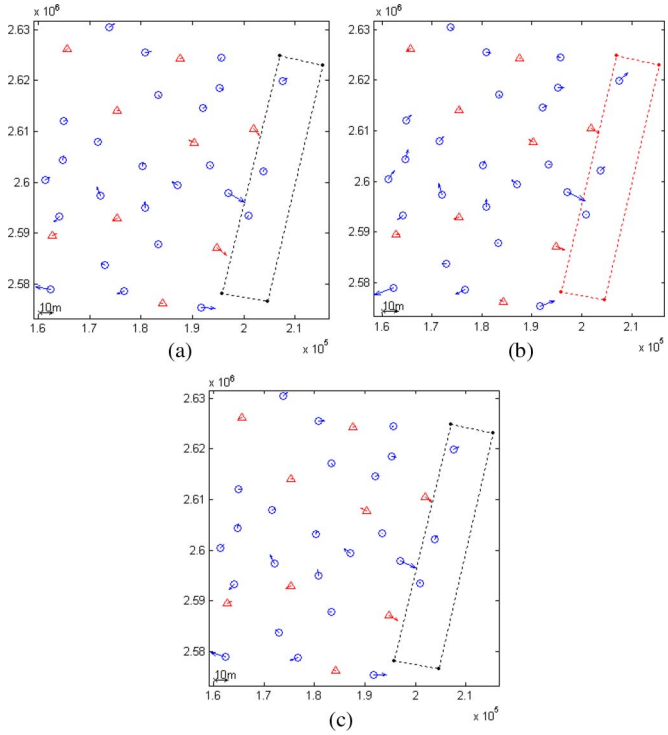

Fig. 10. Error vectors for strip 1 (case I). (a) DG. (b) MBA. (c) RFM.

difference and the error direction is similar. The points near the overlapping area are affected by the constraint on the TPs.

The results of block adjustment are shown in Table VI. The error vector of strips 1, 2, and 3 (after block adjustment) are shown in Figs. 10–12. Triangles indicate the GCPs, while circles represent the ICPs. A DEM is applied to overcome the weak geometric correlation. The results from these three block adjustment methods are quite consistent (except for RFM, strip 3). The absolute accuracy of the block adjustment does not improve. This phenomenon is particularly obvious for strips 2 and 3, where the terrain is steep. The DEM error, with a 40-m resolution, could cause deterioration of the block adjustment results. The slope of the terrain in some of the test areas exceeds 70°.

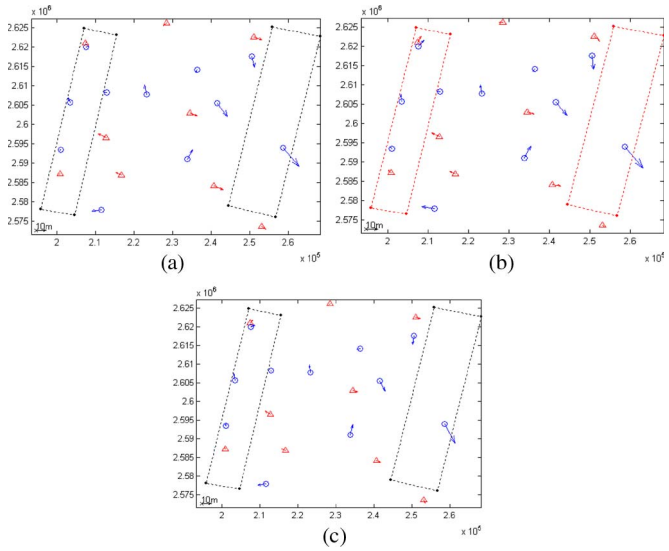

Fig. 11. Error vectors for strip 2 (case I). (a) DG. (b) MBA. (c) RFM.

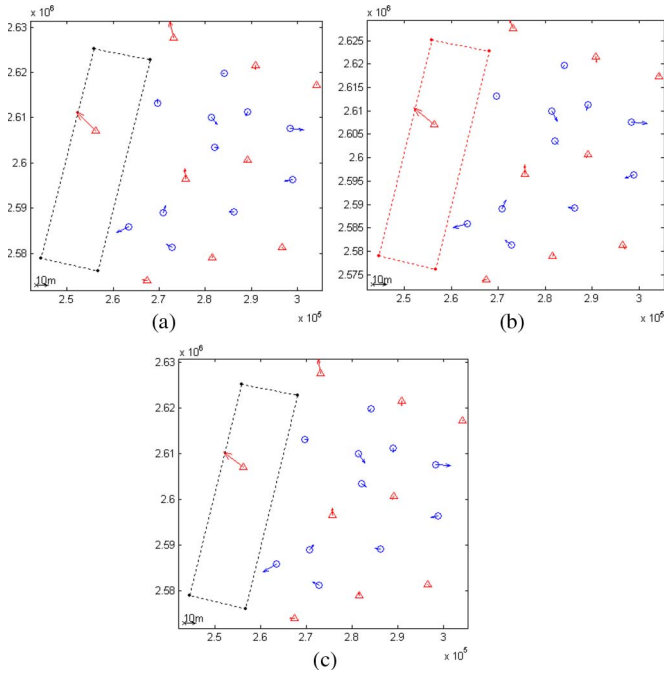

Fig. 12. Error vectors for strip 3 (case I). (a) DG. (b) MBA. (c) RFM.

Case II: The absolute accuracy results obtained with the three single strip adjustment methods for case II are shown as Table VII. The same GCPs and ICPs are applied with each method for comparison. The numbers of GCPs and ICPs are also indicated in the table. The performance of these three methods for the three strips is very similar. The difference of ICP is less than 1 m between the three models, which means that for single image adjustment, they may provide similar results. The absolute accuracy of these three strips ranges from 3.0 to 6.0 m.

The results of block adjustment with DEM control are provided in Table VIII. In addition to the GCP, we also include the TPs used for image stitching. Comparing Tables VII and VIII, we see that the results of block adjustment are similar to those of single strip adjustment for strips 1, 2, and 3. The geometrical

TABLE VII
COMPARISON OF ABSOLUTE ACCURACY FOR SINGLE STRIP ADJUSTMENT (CASE II)

Units: meters	Strip1 No. GCP= 20 No. ICP = 48		Strip2 No. GCP= 22 No. ICP = 31		Strip3 No. GCP= 22 No. ICP = 28	
MBA	**RMSE E**	**RMSE N**	**RMSE E**	**RMSE N**	**RMSE E**	**RMSE N**
GCP	2.31	2.34	3.29	3.58	3.27	5.73
ICP	3.45	3.09	3.76	5.57	5.05	5.28
DG	**RMSE E**	**RMSE N**	**RMSE E**	**RMSE N**	**RMSE E**	**RMSE N**
GCP	2.75	3.06	4.03	4.19	3.87	6.58
ICP	3.37	3.20	3.87	5.57	5.03	5.25
RFM	**RMSE E**	**RMSE N**	**RMSE E**	**RMSE N**	**RMSE E**	**RMSE N**
GCP	3.10	3.02	5.49	5.17	4.01	7.24
ICP	3.24	3.11	4.20	5.97	5.42	4.20

TABLE VIII
COMPARISON OF ABSOLUTE ACCURACY WITH BLOCK ADJUSTMENT (CASE II)

Units: meters	Strip1 No. GCP= 20 No. ICP = 48 No. TP = 32		Strip2 No. GCP= 22 No. ICP = 31 No. TP = 58		Strip3 No. GCP= 22 No. ICP = 28 No. TP = 26	
MBA	**RMSE E**	**RMSE N**	**RMSE E**	**RMSE N**	**RMSE E**	**RMSE N**
GCP	2.73	2.62	4.72	4.82	4.82	6.91
ICP	3.79	2.97	4.82	7.12	4.94	5.39
DG	**RMSE E**	**RMSE N**	**RMSE E**	**RMSE N**	**RMSE E**	**RMSE N**
GCP	3.08	3.87	5.78	5.28	5.14	7.87
ICP	3.52	3.00	5.33	6.84	4.48	4.66
RFM	**RMSE E**	**RMSE N**	**RMSE E**	**RMSE N**	**RMSE E**	**RMSE N**
GCP	3.01	3.47	5.19	5.13	4.70	7.61
ICP	3.56	2.91	4.51	6.50	4.63	4.73

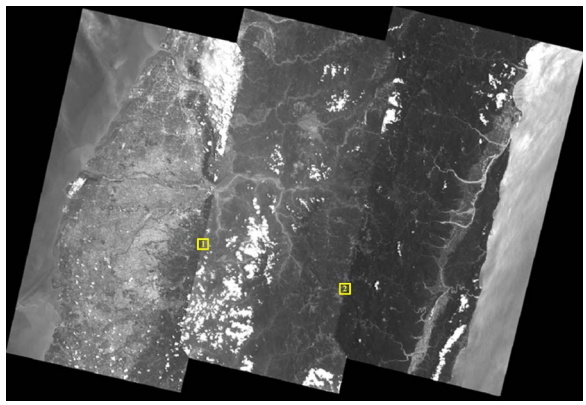

Fig. 13. Mosaic image obtained by block adjustment without gray value balancing.

performance of block adjustment is less than for single strip adjustment. This phenomenon is similar to case I. This could be due to the influence of the coarse DEM for the steep area.

C. Image Mosaicking

The results obtained with the three methods are consistent. We select one case, i.e., case II, and the modified bundle

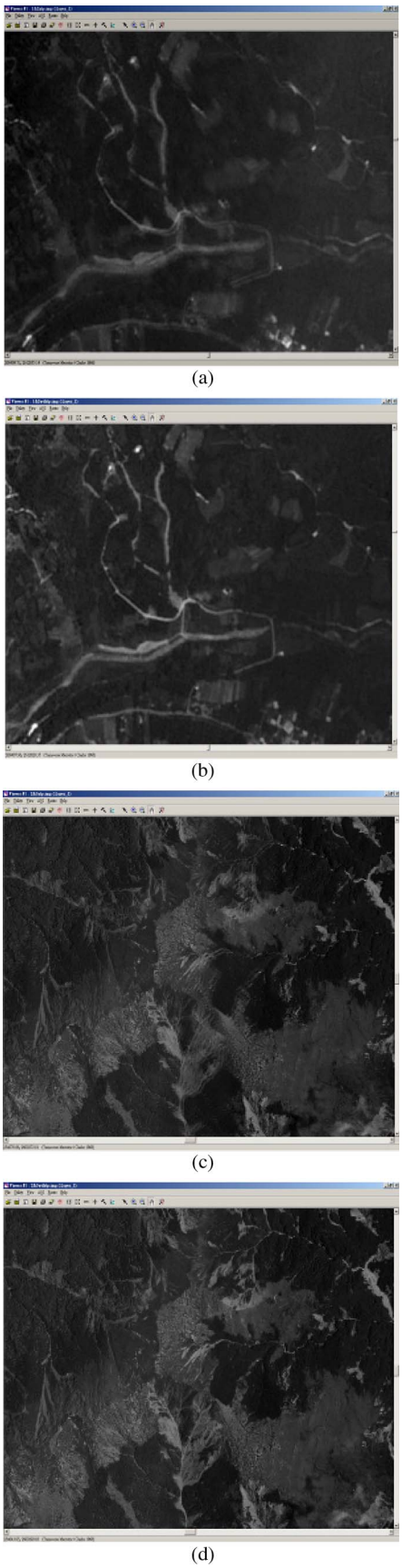

Fig. 14. Comparison of independent and block adjustment for mosaic images. (a) Results of single image adjustment in area 1. (b) Results of block adjustment in area 1. (c) Results of single image adjustment in area 2. (d) Results of block adjustment in area 2.

adjustment method and examine the geometrical consistency of the image mosaicking. The locations of the mosaicked images with respect to the block are shown in Fig. 13. For ease of comparison, two enlargements are shown in Fig. 14. In Fig. 14(a), we find obvious discontinuity. This condition is significantly improved in Fig. 14(b)–(d), where it is also show that the block adjustment may improve the geometrical consistency.

D. Summary of the Experimental Results

The experimental results are summarized as follows.

1) The geometric performances of the three proposed methods are similar.
2) The proposed methods offer significant improvement in the geometric consistency between overlapping images with respect to the single image adjustment by about a factor of 5.
3) The RMSE of ICPs increases slightly when block adjustment is employed.
4) It is expected that in extremely rough mountain areas, the DEM will be less accurate than the GCPs and ICPs. This could explain the improvement in geometric with the deterioration of the RMSE of the check points. Nevertheless, the payoff reveals the effectiveness of the block adjustment process.

IV. Conclusion

In this paper, we have compared three approaches to block adjustment for satellite images with weak convergence geometry using DEM as the elevation control. The first method is a revised version of traditional bundle adjustment. The second is based on the direct georeferencing approach. The third is an RFM with sensor-oriented RPCs. The experimental results indicate that the proposed DEM elevation control method can significantly improve the geometric accuracy as well as reduce discrepancies. The range of improvement is from 3 to 24 m in different cases. The results from the three block adjustment methods are consistent. Tests indicate that the proposed method should be feasible for real applications.

The resolution of the DEM in this study is 40 m, which is not favorable for mountain areas. If the quality of the DEM is improved, higher accuracy may be expected. In future work, more data sets will be validated when DEMs with better quality are available. In this investigation, we use the multiple images taken from a single satellite. Since many other satellites are available, block adjustment with different sensors becomes an important work. The future research will focus on the integration of heterogeneous sensor models.

References

[1] A. Bouillon, M. Bernard, P. Gigord, A. Orsoni, V. Rudowski, and A. Baudoin, "SPOT 5 HRS geometric performances: Using block adjustment as a key issue to improve quality of DEM generation," *ISPRS J. Photogramm. Remote Sens.*, vol. 60, no. 3, pp. 134–146, May 2006.

[2] L. C. Chen and L. H. Lee, "Rigorous generation of digital orthophotos from SPOT images," *Photogramm. Eng. Remote Sens.*, vol. 59, no. 5, pp. 655–661, May 1993.

[3] T. Westin, "Precision rectification of SPOT imagery," *Photogramm. Eng. Remote Sens.*, vol. 56, no. 2, pp. 247–253, Feb. 1990.

[4] A. Habib, S. W. Shin, K. Kim, C. Kim, K. I. Bang, E. M. Kim, and D. C. Lee, "Comprehensive analysis of sensor modeling alternatives for high resolution imaging satellites," *Photogramm. Eng. Remote Sens.*, vol. 73, no. 11, pp. 1241–1251, Nov. 2007.
[5] R. Passini, A. Blades, and K. Jacobsen, "Handling of large block of high resolution space images," *Int. Arch. Photogramm. Remote Sens.*, vol. 36, no. 1/W3, 2005, CD-ROM.
[6] L. C. Chen, T. A. Teo, and J. Y. Rau, "Adaptive patch projection for the generation of orthophotos from satellite images," *Photogramm. Eng. Remote Sens.*, vol. 71, no. 11, pp. 1321–1327, Nov. 2005.
[7] T. Weser, F. Rottensteiner, J. Willneff, J. Poon, and C. S. Fraser, "Development and testing of a generic sensor model for pushbroom satellite imagery," *Photogramm. Rec.*, vol. 23, no. 123, pp. 255–274, Sep. 2008.
[8] J. Grodecki and G. Dial, "Block adjustment of high-resolution satellite image described by rational function," *Photogramm. Eng. Remote Sens.*, vol. 69, no. 1, pp. 59–68, Jan. 2003.
[9] A. B. Orun and K. Natarajan, "A modified bundle adjustment software for SPOT imagery and photography: Tradeoff," *Photogramm. Eng. Remote Sens.*, vol. 60, no. 12, pp. 1431–1437, Dec. 1994.
[10] K. Jacobsen, "Geometric modelling of linear CCDs and panoramic imagers," in *Advances in Photogrammetry, Remote Sensing and Spatial Information Science: 2008 ISPRS Congress Book*. New York: Taylor & Francis, 2008, pp. 145–155.
[11] S. Kocaman and A. Gruen, "Orientation and self-calibration of ALOS PRISM imagery," *Photogramm. Rec.*, vol. 23, no. 123, pp. 323–340, Sep. 2008.
[12] T. Toutin, "Three-dimensional topographic mapping with ASTER stereo data in rugged topography," *IEEE Trans. Geosci. Remote Sens.*, vol. 40, no. 10, pp. 2241–2247, Oct. 2002.
[13] P. E. Miller, M. Kunz, J. P. Mills, M. A. King, T. Murray, T. D. James, and S. H. Marsh, "Assessment of glacier volume change using ASTER-based surface matching of historical photography," *IEEE Trans. Geosci. Remote Sens.*, vol. 47, no. 7, pp. 1971–1979, Jul. 2009.
[14] T. Toutin, "Block bundle adjustment of IKONOS in-track image," *Int. J. Remote Sens.*, vol. 24, no. 4, pp. 851–857, Feb. 2003.
[15] T. Toutin, "Spatiotriangulation with multisensory HR stereo-images," *IEEE Trans. Geosci. Remote Sens.*, vol. 44, no. 2, pp. 456–462, Feb. 2006.
[16] S. Riazanoff, *SPOT Satellite Geometry Handbook*. Toulouse, France: SPOT Image, Jan. 2002.
[17] T. Kim, H. Kim, and S. Rhee, "Investigation of physical sensor models for modeling SPOT 3 orbits," *Photogramm. Rec.*, vol. 22, no. 119, pp. 257–273, Sep. 2007.
[18] S. Leprince, S. Barbot, F. Ayoub, and J. P. Avouac, "Automatic and precise orthorectification, coregistration, and subpixel correlation of satellite images, application to ground deformation measurements," *IEEE Trans. Geosci. Remote Sens.*, vol. 45, no. 6, pp. 1529–1558, Jun. 2007.
[19] E. M. Mikhail and F. Ackermann, *Observation and Least Squares*. New York: Univ. Press Amer., 1982.
[20] C. V. Tao and Y. Hu, "A comprehensive study of the rational function model for photogrammetric processing," *Photogramm. Eng. Remote Sens.*, vol. 67, no. 12, pp. 1347–1357, Dec. 2001.
[21] C. S. Fraser and H. B. Hanley, "Bias compensation in rational function for IKONOS satellite imagery," *Photogramm. Eng. Remote Sens.*, vol. 69, no. 1, pp. 53–57, Jan. 2003.
[22] R. Li, F. Zhou, X. Niu, and K. Di, "Integration of IKONOS and QuickBird imagery for geopositioning accuracy analysis," *Photogramm. Eng. Remote Sens.*, vol. 73, no. 9, pp. 1067–1074, Sep. 2007.
[23] A. Bouillon, E. Breton, L. Lebegue, D. Leger, and A. Meygret, *SPOT Image Quality Performance*. Paris, France: CNES, 2004.
[24] L. C. Chen, T. A. Teo, and J. L. Liu, "The geometrical comparisons of RSM and RFM for FORMOSAT-2 satellite images," *Photogramm. Eng. Remote Sens.*, vol. 72, no. 5, pp. 573–579, May 2006.

Tee-Ann Teo received the M.S.E. and Ph.D. degrees from the National Central University, Taoyuan, Taiwan, in 2002 and 2008, respectively.

He was with the Center for Space and Remote Sensing Research, National Central University, as a Postdoctoral Research Fellow in 2008. He is currently an Assistant Professor with the Department of Civil Engineering, National Chiao Tung University, Hsinchu, Taiwan. His research activities are focused on cyber city modeling, geometrical data processing for remotely sensed data, and lidar processing.

Liang-Chien Chen received the M.S.E. degree from the National Cheng Kung University (NCKU), Tainan, Taiwan, in 1974 and the Ph.D. degree from the University of Illinois, Urbana, in 1985.

He was with the Institute of Photogrammetry, NCKU, from 1985 to 1986. Since 1986, he has been a Professor with the Center for Space and Remote Sensing Research, National Central University, Taoyuan, Taiwan. He is in charge of the Digital Photogrammetry Laboratory and the Earth Resource Satellite Ground Receiving Station. His research activities are focused on the domain of digital photogrammetry, geometrical data processing for remotely sensed data, image feature extraction, lidar processing, and terrain analysis.

Chien-Liang Liu received the B.S. and M.S.E. degrees from the National Central University, Taoyuan, Taiwan, in 2002 and 2004, respectively.

Since 2004, he has been an Associate Research Engineer with the Center for Space and Remote Sensing Research, National Central University. His research activities are mostly concentrated in the domain of geometrical data analysis for linear array sensors.

Yi-Chung Tung received the B.S. and M.S.E. degrees from the National Central University, Taoyuan, Taiwan, in 2003 and 2005, respectively.

After completing military service, he joined a work and travel program to Australia in 2008. He is currently an Engineer with the CECI Engineering Consultants, Inc., Taipei, Taiwan. His research interests include photogrammetry and GIS data analysis.

Wan-Yu Wu received the B.S. degree from the National Chengchi University, Taipei, Taiwan, in 2006 and the M.S.E. degree from the National Central University, Taoyuan, Taiwan, in 2008.

Since 2008, she has been an Engineer with the Kingwaytek Technology Company, Ltd., Taipei, Taiwan. Her research interests include GIS data analysis.